This is the post-print i.e. final accepted version of the paper https://doi.org/10.1016/j.nanoen.2020.104495

23.5%-efficient silicon heterojunction silicon solar cell using molybdenum oxide as hole-selective contact

Julie Dréon*, Quentin Jeangros, Jean Cattin, Jan Haschke, Luca Antognini, Christophe Ballif and Mathieu Boccard

Photovoltaics and Thin-Film Electronics Laboratory (PV-lab), Institute of Microengineering (IMT), École Polytechnique Fédérale de Lausanne (EPFL), Rue de la Maladière 71b, CH-2002 Neuchâtel, Switzerland.

*Corresponding author: julie.dreon@epfl.ch

Keywords: solar cell, silicon heterojunction, molybdenum oxide, carrier-selective contacts, dopant free, thickness variation

Abstract

Interest in silicon heterojunction solar cells is growing due to their manufacturing simplicity and record efficiencies. However, a significant limitation of these devices still stems from parasitic light absorption in the amorphous silicon layers. This can be mitigated by replacing the traditional (p) and (n) doped amorphous silicon selective layers by other materials. While promising results have been achieved using molybdenum oxide (MoO_x) as a front-side hole-selective layer, charge transport mechanisms in that contact stack have remained elusive and device efficiencies below predictions. We carefully analyze the influence of the MoO_x and intrinsic a-Si:H thicknesses on current-voltage properties and discuss transport and performance-loss mechanisms. In particular, we find that thinning down the MoO_x and (i)a-Si:H layers (down to 4 nm and 6 nm respectively) mitigates parasitic optical sub-bandgap MoO_x absorption and drastically enhances charge transport, while still providing excellent passivation and selectivity. High-resolution transmission microscopy reveals that such thin MoO_x layer remains continuous and close to a MoO_3 stoichiometry in spite of the reactive sputtering and annealing steps involved in the electrode deposition. A screen-printed device reaching a certified efficiency of 23.5% and a fill factor of 81.8% is demonstrated, bridging the gap with traditional Si-based contacts and demonstrating that dopant-free selective contacts can rival traditional approaches.

Introduction

The interest in silicon heterojunction (SHJ) is growing in the field of photovoltaics due to the simplicity of their structure and processing, as well as the high efficiencies that can be achieved [1], [2]. The record efficiency for a silicon single junction is currently held by a SHJ combined with an interdigitated back contacted (IBC) design, reaching 26.7% [3], [4]. Most of the SHJs use stacks of intrinsic and doped hydrogenated amorphous silicon (a-Si:H) as passivating and carrier-selective layers [5]. These stacks provide good surface passivation and selectivity thanks to the high hydrogen content of these layers and dopability of amorphous silicon, respectively [1], [6]–[8].

However, the excellent passivation performance of this contact architecture often comes at the expense of carrier transport in comparison with solar cells based on silicon homojunctions which translate into fill factor (FF) losses. This effect stems from the lower conductivity of doped a-Si:H compared to crystalline silicon, band offsets between these two crystalline phases [9][10], and the formation of an opposing Schottky contact between a-Si:H and the transparent conductive oxide (TCO) [11]–[13]. In addition, the use of a-Si:H (bandgap of ~1.7 eV) on the light-incoming side of the device leads to parasitic absorption below 500 nm [1], [14]. Photons that are parasitically absorbed in the intrinsic a-Si:H ((i)a-Si:H) can partly contribute the cell's short circuit current density (J_{sc}), but photons absorbed in the doped a-Si:H layer are lost [14], [15]. This typically causes a J_{sc} loss of up to 2.1 mA cm^{-2} compared to the one of a cell with an ideal cell front-side [15]. One investigated strategy to overcome this parasitic absorption is to replace the intrinsic and p-type (i/p)a-Si:H layers by more transparent carrier selective contacts. Silicon-based materials (in their nanocrystalline phase and/or alloyed with carbon and oxygen) [16]–[21], and transition metal oxides (TMOs) [22]–[27] are the most widely followed approaches, alongside a few other organic and inorganic materials [28], [29].

Most efficient devices using non-Si contacts have been achieved with molybdenum oxide (MoO_x) as hole-selective contact [30]–[32]. This ~3.0-eV-bandgap material substitutes p-type a-Si:H on the light-incoming side of the solar cell to reduce parasitic absorption at short wavelengths [23], [26], [30], [33]–[35]. The high workfunction of MoO_x (5.7 eV to 6.9 eV [22], [26], [33], [36], [37]) enables this n-type semiconductor to ensure hole selectivity for a silicon absorber. Yet it does not provide sufficient surface passivation when deposited directly on c-Si [38]. An (i)a-Si:H layer is thus usually inserted as sketched in Fig 1a.

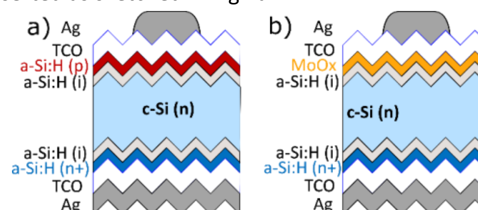

Figure 1: a) standard SHJ and b) MoOx-based cell schema

As for standard SHJ devices (see Fig. 1b), a transparent electrode is required to provide lateral transport of charges on the positive-electrode side. A remarkable 22.5%-efficient device (with an FF of 80%) was demonstrated in 2015 using a combination of (i)a-Si:H, MoO_x, hydrogen-doped indium oxide and a copper-plated grid [30]. Efficiency and FF were on par with those of standard SHJ state-of-the art values at the time [39].

However, there are still challenges when contacting c-Si with a (i)a-Si:H/MoOx/TCO stack. First, a strong degradation of hole extraction, characterized by an FF drop, occurs upon annealing above 130 °C, a temperature required to cure industrial screen-printing pastes. Such degradation was attributed to the formation of an interlayer between MoO_x and TCO [30], the formation of SiO_x at the MoO_x/a-Si:H interface [40], or/and the reduction of MoO_x by H effusing from adjacent layers leading to a decrease of its workfunction [41]. The latter could be successfully mitigated by reducing the H-content of the a-Si:H layer prior to MoO_x deposition, improving efficiency by $2\%_{absolute}$ yet without reaching similar performances as best-in-class devices [41].

Second, sub-bandgap absorption in the MoO_x-based contact stack hampers its transparency and thus its advantage over standard (p)a-Si:H [30], [40]. Reducing the MoO_x thickness is therefore a promising strategy, especially since TMOs have been reported to better protect (i)a-Si:H layers from damage induced by TCO sputtering compared to (p)a-Si:H [40], [42]–[45]. However, since electrical transport in the MoO_x layer is carried by electrons through defect states, the MoO_x/(i)a-Si:H interface is expected to be more recombining than the (p)a-Si:H /(i)a-Si:H one. This could affect passivation, and call for a thicker (i)a-Si:H layer than when using a (p)a-Si:H contact.

Following these considerations, we vary here the thicknesses of the (i)a-Si:H and MoO_x layers in SHJ devices and discuss their influence on the optical and electrical performance of the cell. Furthermore, a low temperature curing paste is employed to avoid degradation and to assess the potential of this contact strategy using state-of-the-art SHJ processing [41], [46].

Experimental details

Fig. 2 details the processing sequence followed here. We used nine 180-µm-thick n-type textured float zone wafers with a resistivity of 1.7-2.3 Ω cm. A stack composed of (i)a-Si:H /(n)aSi:H /(n)µc-Si:H was deposited at the back side by plasma enhanced chemical vapor deposition (PECVD) at 200 °C on all wafers. Three different thicknesses[1] (6 nm, 8 nm and 10 nm) of (i)a-Si:H were then deposited on the front side of the wafers (three co-processed wafers per thickness). Annealing in air at 250 °C during 20 min, prior to MoO_x deposition, was then performed in an oven ("pre-annealing" step [41]) to reduce the hydrogen content in the front-side (i)a-Si:H layer. The pre-annealing step was shown to induce no detectable thickness variation by ellipsometry. After removal of the surface oxide in an aqueous solution of 1% diluted hydrofluoridric acid (HF), a 4-nm-, 8-nm- or 9-nm-thick MoO_x layer was thermally evaporated on the front side, each time on three wafers with a different (i)a-Si:H thickness. MoO_x evaporation was done in a vacuum chamber (base pressure before deposition ~ $4*10^{-6}$ mbar) from stoichiometric MoO_3 powder at a deposition rate of about 0.03 nm/s. Finally, indium tin oxide (ITO) was sputtered on the front (70 nm) through a mask to form five 2 x 2 cm^2 devices per wafer. ITO (150 nm) and Ag (100 nm) were then sputtered over the full back side area. For these steps, only wafers with the same MoO_x thickness (thus three wafers each time) were co-processed. A silver grid was finally screen-printed on the front side using a low-temperature paste, cured at 130 °C. In the front metallization design, busbars define the perimeter of the cells and are excluded from the measurement area.

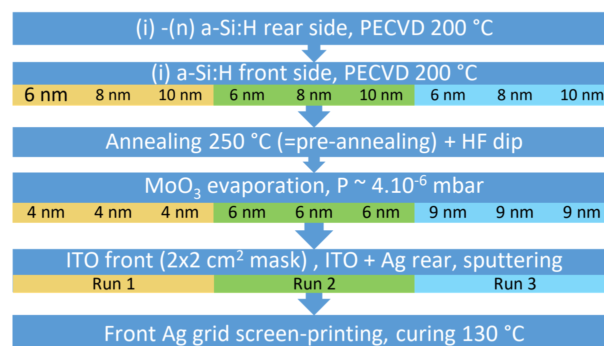

Figure 2: Process flow

Standard SHJ solar cells were processed as references, using the same rear side stack, a 6-nm-thick (i)a-Si:H layer on the front side capped with an 8-nm-thick PECVD (p)a-Si:H layer instead of evaporated MoO_x, omitting the pre-annealing step since it is useful to avoid H effusion in MoOx only, and as it generally leads to a slight passivation degradation. Standard screen-printing Ag paste cured at 210 °C was used.

The structure and chemistry of the contact was assessed by transmission electron microscopy (TEM). For that purpose, a layer stack of (i)a-Si:H/MoO_x/ITO was deposited on a <111>-oriented mechanically polished (n)c-Si wafer. After annealing at 130 °C for 30 minutes, mimicking curing of the low temperature paste, a thicker MoO_x layer (of 20 nm) was deposited on top of ITO to serve as a freshly evaporated MoO_x reference. The contact stack was finalized by sputtering a Ag layer. A thin lamella was prepared using the conventional focused ion beam lift-out technique with a final thinning voltage of 2 kV in a Zeiss Nvision 40. Scanning TEM (STEM) high-angle annular dark-field (HAADF) images and energy-

[1] All thicknesses are given on textured surfaces, calculated from measurements on flat Si or glass divided by a ratio of 1.5 accounting for the pyramids geometry.

dispersive X-ray spectroscopy maps were recorded in a FEI Titan Themis microscope operated at 200 kV with a beam current of 200 pA. Electron energy-loss spectra (EELS) were acquired at 80 kV and at cryogenic temperature (-165 °C) to assess the oxidation states of the thin (4 nm) and thick (20 nm) MoO_x layers without introducing electron beam artifacts [47]. A convergence semi-angle of 30.5 mrad was employed, while the collection semi-angle was 47 mrad. A dispersion of 0.1 eV/channel was employed for the dual EELS scans. For comparison purposes, M3 edges were aligned and rescaled to a value of 1 after removing the conventional power law background (using data within the ranges 380-390 eV and 445-450 eV to fit the background). Experimental data was compared to the reference MoO_2 and MoO_3 EELS spectra of [47] to assess the oxidation state of MoO_x as a function of its thickness and processing history.

Results and discussion

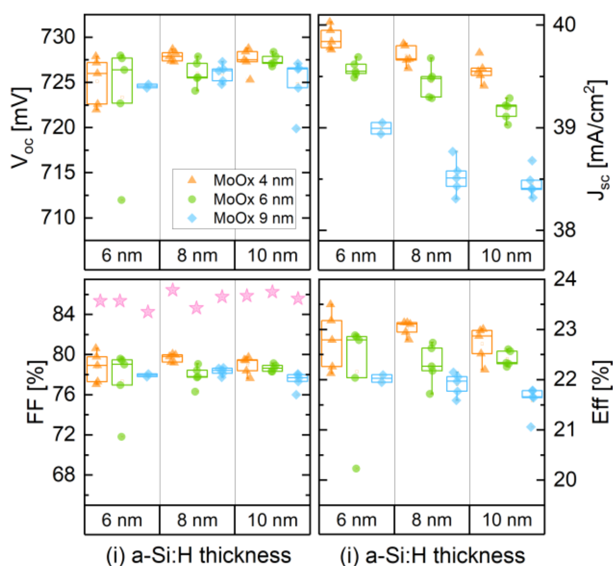

Figure 3: a) Voc, b) J_{sc}, c) FF, d) Efficiency of MoOx-based solar cells with different thicknesses for the front (i)a-Si:H and MoO_x layers. Each dot represents one of five cells on a wafer. One wafer was prepared per condition. The pink stars represent the pseudo FF extracted from the Suns Voc measurements.

Fig. 3 shows the parameters extracted from J-V measurements of the devices with different (i)a-Si:H and MoO_x thicknesses. The measurements were done with a designed black mask shading the external edges of the cell and the entire inactive area of the wafer. The open circuit voltage (V_{oc}) values in Fig. 3a are similar for all MoO_x and (i)a-Si:H thicknesses. Yet, statistical analysis indicates a statistically relevant V_{oc} gain upon thickening the (i)a-Si:H layer of 0.61 ± 0.27 mV/nm (see Supporting Information about statistical analysis) and a V_{oc} loss of -0.41 ± 0.25 mV/nm when changing the MoO_x thickness, but in that case, statistical analysis suggests the trend is less clear. No correlation between the two thicknesses influence on V_{oc} is observed. The thinnest MoO_x thus globally yields a V_{oc} ~2 mV higher than for the thickest layers. Part of this gain (0.6 mV) can be attributed to the photogeneration difference, as estimated using a one-diode model with J_{sc} shown in Fig. 3b as the photogenerated current, but photoluminescence imaging (Fig. S1 in Supporting Information) and high illumination V_{oc} measurements (Fig. S2) [8] suggest that the thinnest MoO_x also provides better passivation and selectivity than thicker films (discussed in Supporting Information). This demonstrates that the 4 nm MoO_x film is sufficiently thick to protect the passivation provided by the (i)a-Si:H layer from sputtering damage and maintains sufficient selectivity to efficiently extract holes.

Fig. 3b shows that J_{sc} decreases when thickening either the MoO_x or (i)a-Si:H layer. The optical loss induced by MoO_x (0.25 ± 0.01 mA cm^{-2} per nm of MoO_x thickness, irrespective of the (i)a-Si:H thickness in the range tested) is higher than that induced by (i)a-Si:H (0.10 ± 0.01 mA cm^{-2} per nm of a-Si:H, irrespective of the MoO_x thickness, and as reported in Ref. [15]).
To identify more accurately the origin of these losses, external quantum efficiency (EQE) and reflectance measurements are shown in Fig. 4 and Table 1, highlighting gains in J_{sc} compared to the reference (p)a-Si:H SHJ cell. Reflectance is similar for all MoO_x devices, with the exception of a slight variation in the 400-600 nm range, which may originate from batch-to-batch ITO variations. From Fig. 4a, the (i)a-Si:H thickness influences absorption mostly for wavelengths below 600 nm, and has no effect on reflection. On the other hand, Fig. 4b shows that the use of MoO_x influences absorption over the whole wavelength range. Noticeably, the EQE signal is reduced from 600 nm to 1200 nm when increasing the MoO_x thickness. This is due to sub-bandgap parasitic absorption in this range, as previously observed in Refs. [30], [40]. The fact that this effect occurs in the visible range may also explain why MoO_x sub-bandgap absorption impacts the J_{sc} more strongly than (i)a-Si:H UV-blue absorption, as the photon flux is lower in the UV. In our study, a J_{sc} loss of 0.4 mA cm^{-2} in the 600-900 nm range is recorded for the thickest MoO_x, but interestingly no loss is observed for the thinnest MoO_x. An internal quantum efficiency comparison in Fig. S3 yet suggests that sub-bandgap parasitical absorption is still slightly present for this film. In the 320-600 nm range, gains in J_{sc} vary from 0.5 to 0.8 mAcm^{-2} depending on the MoO_x thickness (see Table 1). Although larger J_{sc} gains compared to standard SHJ cells were reported in literature in this range (1.9 mA cm^{-2} in [34], 1.3 mA m^{-2} in [23], and 0.9 mA cm^{-2} in [30]), these gains were mitigated by a strong loss at longer wavelengths, reducing the overall J_{sc} gain. In Ref. [34], the replacement of ITO by more transparent IO:H presumably compensated losses associated with sub-bandgap absorption in the MoO_x layer. Overall, cells featuring the thinnest MoO_x film investigated in this study exhibit a J_{sc} gain of 1.3 mA cm^{-2}. These results demonstrate that an adequate

device architecture enables to fully benefit from the improved transparency of MoO_x compared to (p)a-Si:H.

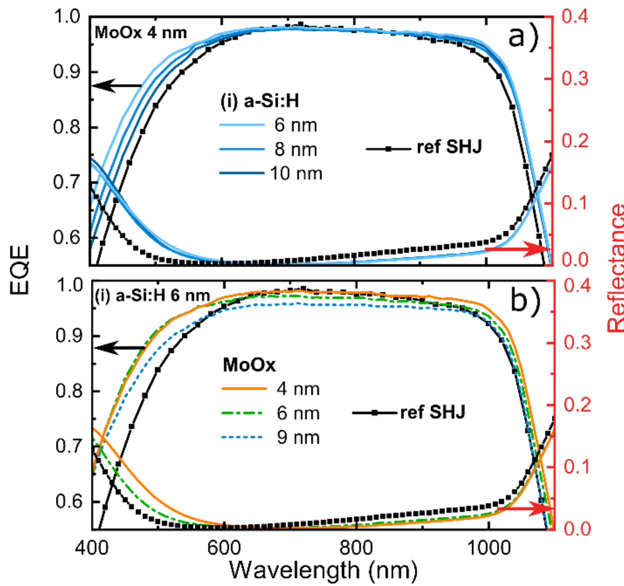

Figure 4: EQE and reflectance of a) devices with 4 nm MoOx and variable (i)a-Si:H thickness; b) devices with 6 nm (i)a-Si:H and variable MoO_x thickness.

Samples with thinnest (i)a-Si:H (6 nm)	J_{sc} gain or loss (mA/cm^2)			
	320 to 600 nm	600 to 900 nm	900 to 1180 nm	Total
MoO_x 4 nm	0.84	0.03	0.46	1.33
MoO_x 6 nm	0.83	-0.16	0.27	0.94
MoO_x 9 nm	0.53	-0.43	0.05	0.15

Table 1: J_{sc} gain for MoOx-based cells compared to the reference SHJ cell over various wavelength ranges calculated from EQE curves.

Fig. 3c shows that the thinnest layers investigated here are sufficient to ensure efficient charge extraction and passivation as a FF of up to 81% is achieved for the thinnest combination of MoOx and (i)a-Si:H layers. Statistical analysis indicates a stronger influence of the MoOx thickness, with a FF loss of -0.3 ± 0.1 %/nm and no significant impact from the (i)a-Si:H thickness. In the case of a standard SHJ with (p)a-Si:H, the (i)a-Si:H thickness affects the FF significantly [15], suggesting that the MoO_x layer imposes stronger selectivity than the (p)a-Si:H one. Indeed, if MoO_x is more selective (thanks to its higher workfunction compared to (p)a-Si:H [23]), the hole population in (i)a-Si:H would be larger, which should lower the FF dependency on (i)a-Si:H thickness.

For standard SHJ solar cells, it is reported that an increase in (p)a-Si:H thickness leads to a higher FF [13], [15], [48], which might be due to the screening effect provided by the (p)a-Si:H layer thickness ("screening length") towards the reverse Schottky diode induced at the interface ITO/(p)a-Si:H due to work function mismatch [13]. The same trend for FF was observed by increasing the p-type layer doping [49]. Increasing the MoO_x thickness, however, leads to a drop in FF, which suggest that MoO_x contact behaves differently. This might be due to its n-type character, preventing the formation of a Schottky contact with ITO (as is the case with (p)a-Si:H which is depleted due to the workfunction mismatch between the (p)-type a-Si:H and the (n)-type ITO). This FF drop is linked to an increase of the cell series resistance (R_s), notably due to the thicker MoOx film (Fig. S4). On glass samples with 8-nm sub-stoichiometric MoO_x, we measured a resistivity of $4.5*10^4$ Ω cm after evaporation, and 300 Ω cm after annealing at 180°C, literature values span from 200 Ω cm [50] to $5*10^4$ Ω cm [51]. This leads to an increase of 0.005 R_s / 1 nm MoO_x (taking a MoOx resistivity of $4.5*10^4$ Ω cm), which is too low to explain the FF decrease. This confirms other studies suggesting that transport is not only limited by ohmic losses only in this kind of contact [52].

All these cells showed remarkable stability after 11 months of unencapsulated storage in air with less than 1 mV change in Voc and FF fluctuation within +/-1% (see data in SI, Fig. S5).

Fig. 5 shows the J-V plots of cells with different MoO_x thicknesses. We observe a non-linear characteristic, usually referred to as "s-shape," which is typical for solar cells with unoptimized passivating contacts. This effect arises when the extraction rate of majority carriers of the contact becomes limited at this contact, or when the leakage rate of these carriers at the opposite contact is not negligible [53]. Although thinning down the MoO_x layer mitigates this effect, it is still present in the thinnest layer as evidenced by the lower current at high forward voltages compared to the reference SHJ. The impact on cell performance is however small, as the reference SHJ and the thinnest MoO_x cells (orange) have a similar characteristic in the fourth quadrant. The higher J_{sc} of the cells with a thin MoO_x leads to a higher efficiency compared to the reference SHJ cell.

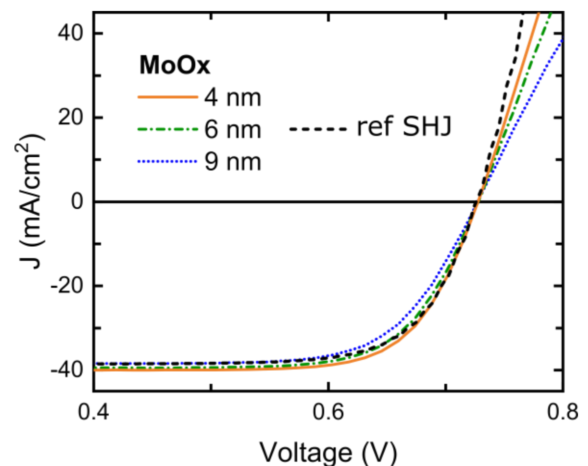

Figure 5: J-V of the three different cells featuring different MoOx thicknesses, with 6 nm of (i)a-Si:H for all devices. The dashed black line represents the reference SHJ cell ((p) a-Si:H of 8 nm, (i) a-Si:H of 6 nm).

The microstructural and chemical properties of MoO_x were investigated by STEM HAADF imaging and EDX, as shown in Fig. 6a-c, to check MoO_x contact oxidation state and aspect in the device. The EDX line profile shown in Fig. 6c highlights the presence of a thin amorphous SiO_x layer at the (i)a-Si:H/MoO_x interface, as reported in [40]. This layer is too thick (more than 2 nm) to be attributed to a native oxide prior to MoO_x deposition since an HF dip is included in the process around 20 min before samples loading in evaporator vacuum chamber. The Mo M3-M2 EELS fine structure of the thin MoO_x contact layer is comparable to the one of the thicker reference MoO_x layer (~20-nm-thick) that was not subject to any annealing or plasma exposure (Fig. 6d-f). These MoO_x EELS spectra indicate that the layers have a stoichiometry closer to MoO_3 than MoO_2, even for a layer as thin as 4 nm and sandwiched between a-Si:H and ITO and subjected to annealing at 130 °C which could reduce it by hydrogen effusion from the a-Si:H layer. Either the MoO_x stoichiometry is indeed unchanged (compared to the substoichiometric MoO_x reference) by its surroundings, or the higher affinity of Si to Mo does result in a MoO_x reduction after deposition (leading to the observed interfacial SiO_x layer), which is cancelled by the subsequent plasma exposure during ITO deposition which could induce its re-oxidation. The main conclusion we can draw from this study is that the thin 4 nm MoOx embed in the contact stack has an oxidation state similar to the thick reference one.

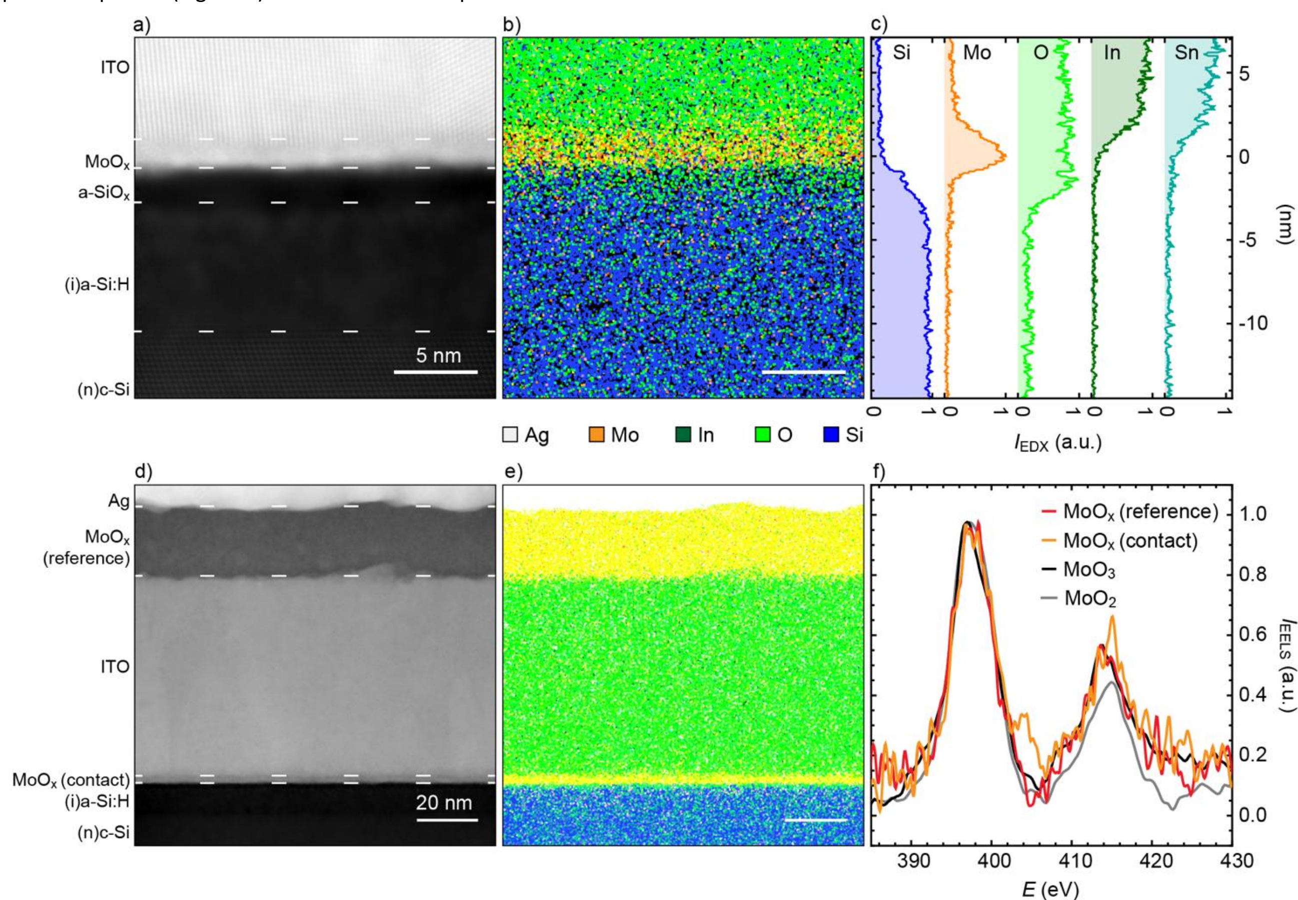

Figure 6: a) STEM HAADF image of the (i)a-Si:H/MoO_x/ITO contact deposited on a <111>-oriented (n)c-Si wafer, b) corresponding EDX map and c) background-subtracted EDX line profiles of the Si K, O K, In L, Sn L edges. d) STEM HAADF image of the contact coated with an as-deposited MoO_x layer/Ag stack, e) corresponding EDX map and f) EELS Mo M3-M2 edges of the thin and thick MoO_x layers compared to reference spectra.

Optimized MoO_x contact design for record performance

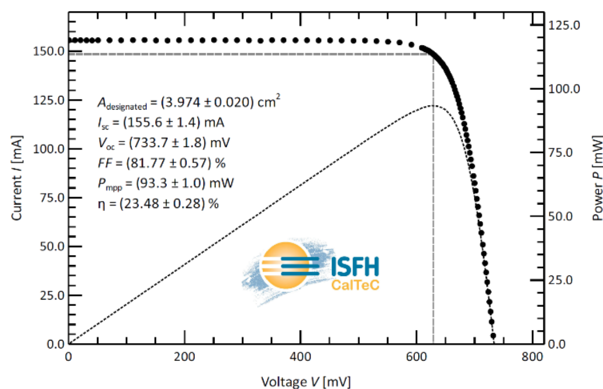

Fig. 8: certified J-V and power plots of the best MoO_x-based cell processed in the lab (certified by ISFH)

The highest efficiency of this series was obtained for a 4-nm-thick MoO_x layer and a 6-nm-thick (i)a-Si:H film. Given that results with the thinnest (i)a-Si:H are quite spread, we processed another 4-nm MoOx cells with thicker (i)a-Si:H layer of 8 nm, and a obtained a certified efficiency of 23.5% (Fig. 8), with a remarkable FF close to 82%. This record efficiency for such solar cell was obtained without any masking step or photolithography and used a low-temperature Ag screen-printed metallization, causing ~3% shadowing [46], [54].

The 39.15 mA/cm² current density reached for this record device is significantly below the 44.1 mA/cm² Lambertian limit for a 180-µm-thick silicon wafer. Using the analytical model presented in Ref [55], we estimate that the measured Jsc could be improved by 0.8 mA/cm² by suppressing all absorption in the MoO_x layer and by another 0.8 mA/cm² by suppressing all absorption in the front (i)aSi:H layer. Another 0.8 mA/cm² and 1.2 mA/cm² could be gained by suppressing primary reflection and grid shading, respectively. About 1.2 mA/cm² could be recovered from parasitic absorption in the other layers (front ITO and rear ITO and Ag), and 0.2 mA/cm² from improving light trapping.

Conclusion

In summary, we studied the influence of the thicknesses of the MoO_x and (i)a-Si:H films used as hole contacts in SHJs. The thinnest layers studied here (~4 nm and ~6 nm for MoO_x and (i)a-Si:H, respectively) resulted in best device performances, highlighting that such thin contact stacks enable simultaneously high selectivity, passivation, and good charge carrier transport. Thicker layers were found to lead to higher series resistance or charge carrier selectivity losses, without any strong correlation between the two. The device employing the thinnest MoO_x showed a higher optical response (higher EQE) than the reference (p)a-Si:H-based SHJ over the whole wavelength range (320–1180 nm). This gain in photocurrent of 1.3 mA/cm² resulted from mitigation in parasitic absorption losses. High-resolution transmission electron microscopy imaging and electron energy-loss spectroscopy revealed that the 4-nm-thick evaporated MoO_x layer is continuous and has a stoichiometry close to MoO_3, even after sputtering the overlaying ITO layer and annealing the contact stack. Overall, the high J_{sc} allowed by this contact stack enabled the demonstration of a 23.5%-efficient device, highlighting that MoO_x is an excellent hole contact for c-Si heterojunctions. By reaching a similar efficiency to that of best SHJs cells produced in our laboratory [56], this study demonstrates that MoO_x can rival traditional contacting schemes in spite of its lower level of optimization. It demonstrates that carrier-selective contacts relying on non-Si materials are relevant for high-efficiency silicon photovoltaics. As a perspective, reducing further the thickness of the MoO_x (based on Jsc trends, a 1-nm MoO_x-thick device should have a Jsc higher by 0.7 mA/cm² compared to actual 4-nm MoO_x-thick cells) layer and investigating the industrial feasibility and long term stability of such devices will be necessary steps before large-scale deployment of this technology can be envisaged.

Acknowledgements

The authors would like to thank C. Allebé and P. Wyss for the wafer cleaning and texturization, V. Paratte for processing passivation layers and electron contact on the c-Si wafer, N. Badel for the Ag screen-printing metallization, and Cédric Bucher and Aymeric Schafflützel for technical support.

This project is funded by the Swiss national science fundation under Ambizione Energy Grant ICONS (PZENP2_173627).

[1] S. DeWolf, A. Descoeudres, Z. C. Holman, and C. Ballif, "High-efficiency silicon heterojunction solar cells: A review," *Green*, vol. 2, no. 1, pp. 7–24, 2012.

[2] C. Ballif *et al.*, "Solving all bottlenecks for silicon heterojunction technology," *Photovoltaics Internati*, vol. 42, pp. 85–97, 2019.

[3] K. Yoshikawa *et al.*, "Silicon heterojunction solar cell with interdigitated back contacts for a photoconversion efficiency over 26%," *Nat. Energy*, vol. 2, no. 5, p. 17032, Mar. 2017.

[4] M. A. Green, E. D. Dunlop, D. H. Levi, J. Hohl-Ebinger, M. Yoshita, and A. W. Y. Ho-Baillie, "Solar cell efficiency tables (version 54)," *Prog. Photovoltaics Res. Appl.*, vol. 27, no. 7, pp. 565–575, 2019.

[5] M. Tanaka *et al.*, "Development of New a-Si/c-Si Heterojunction Solar Cells: ACJ-HIT (Artificially Constructed Junction-Heterojunction with Intrinsic Thin-Layer)," *Jpn. J. Appl. Phys.*, vol. 31, no. Part 1, No. 11, pp. 3518–3522, Nov. 1992.

[6] M. Taguchi *et al.*, "HITTM cells?high-efficiency crystalline Si cells with novel structure," *Prog. Photovoltaics Res. Appl.*, vol. 8, no. 5, pp. 503–513, Sep. 2000.

[7] P. G. Le Comber and W. E. Spear, "Electronic transport in amorphous silicon films," *Phys. Rev. Lett.*, vol. 25, no. 8, pp. 509–511, 1970.

[8] M. Bivour *et al.*, "Doped layer optimization for silicon heterojunctions by injection-level-dependent

open-circuit voltage measurements," *IEEE J. Photovoltaics*, vol. 4, no. 2, pp. 566–574, 2014.

[9] A. Shah and W. Beyer, "BASIC PROPERTIES OF HYDROGENATED AMORPHOUS SILICON ({a-Si:H})," in *Thin-Film Silicon Solar Cells*, A. Shah, Ed. EPFL Press, 2010, pp. 17–96.

[10] W. G. J. H. . Van sark, F. Roca, and L. Korte, *Physics and technology of amorphous-crystalline heteronstrutures sillicon solar cells.* 2012.

[11] L. Zhao, C. L. Zhou, H. L. Li, H. W. Diao, and W. J. Wang, "Role of the work function of transparent conductive oxide on the performance of amorphous/crystalline silicon heterojunction solar cells studied by computer simulation," *Phys. Status Solidi Appl. Mater. Sci.*, vol. 205, no. 5, pp. 1215–1221, 2008.

[12] E. Centurioni and D. Iencinella, "Role of front contact work function on amorphous silicon/crystalline silicon heterojunction solar cell performance," *IEEE Electron Device Lett.*, vol. 24, no. 3, pp. 177–179, 2003.

[13] M. Bivour, S. Schröer, and M. Hermle, "Numerical analysis of electrical TCO / a-Si:H(p) contact properties for silicon heterojunction solar cells," *Energy Procedia*, vol. 38, pp. 658–669, Jan. 2013.

[14] A. Paduthol, M. K. Juhl, G. Nogay, P. Löper, A. Ingenito, and T. Trupke, "Impact of different capping layers on carrier injection efficiency between amorphous and crystalline silicon measured using photoluminescence," *Sol. Energy Mater. Sol. Cells*, vol. 187, no. March, pp. 55–60, 2018.

[15] Z. C. Holman *et al.*, "Current Losses at the Front of Silicon Heterounction Solar Cells," *IEEE J. Photovoltaics*, vol. 2, no. No. 1, 2012.

[16] L. Mazzarella, S. Kirner, B. Stannowski, L. Korte, B. Rech, and R. Schlatmann, "P-type microcrystalline silicon oxide emitter for silicon heterojunction solar cells allowing current densities above 40 mA/cm2," *Appl. Phys. Lett.*, vol. 106, no. 2, pp. 0–5, 2015.

[17] L. Mazzarella *et al.*, "Nanocrystalline silicon emitter optimization for Si-HJ solar cells: Substrate selectivity and CO2 plasma treatment effect," *Phys. Status Solidi Appl. Mater. Sci.*, 2017.

[18] A. N. Fioretti, M. Boccard, R. Monnard, and C. Ballif, "Low-Temperature $ p $-Type Microcrystalline Silicon as Carrier Selective Contact for Silicon Heterojunction Solar Cells," *IEEE J. Photovoltaics*, 2019.

[19] D.-W. Kang, P. Sichanugrist, H. Zhang, and M. Konagai, "Wide-bandgap p-type microcrystalline silicon oxycarbide using additional trimethylboron for silicon heterojunction solar cells," *Prog. Photovoltaics Res. Appl.*, vol. 15, no. February 2013, pp. 659–676, 2017.

[20] D. Zhang, D. Deligiannis, G. Papakonstantinou, R. van Swaaij, M. Zeman, and others, "Optical Enhancement of Silicon Heterojunction Solar Cells With Hydrogenated Amorphous Silicon Carbide Emitter," *Photovoltaics, IEEE J.*, vol. 4, no. 6, pp. 1326–1330, 2014.

[21] J. P. Seif *et al.*, "Amorphous silicon oxide window layers for high-efficiency silicon heterojunction solar cells," *J. Appl. Phys.*, vol. 115, no. 2, p. 24502, 2014.

[22] C. Battaglia *et al.*, "Hole Selective MoO," *Nano Lett.*, vol. 14, pp. 967–971, 2014.

[23] M. Bivour, J. Temmler, H. Steinkemper, and M. Hermle, "Molybdenum and tungsten oxide: High work function wide band gap contact materials for hole selective contacts of silicon solar cells," *Sol. Energy Mater. Sol. Cells*, vol. 142, pp. 34–41, 2015.

[24] M. Mews, L. Korte, and B. Rech, "Oxygen vacancies in tungsten oxide and their influence on tungsten oxide/silicon heterojunction solar cells," *Sol. Energy Mater. Sol. Cells*, vol. 158, pp. 77–83, 2016.

[25] L. G. Gerling *et al.*, "Transition metal oxides as hole-selective contacts in silicon heterojunctions solar cells," *Sol. Energy Mater. Sol. Cells*, vol. 145, pp. 109–115, 2016.

[26] J. Meyer, S. Hamwi, M. Kröger, W. Kowalsky, T. Riedl, and A. Kahn, "Transition Metal Oxides for Organic Electronics: Energetics, Device Physics and Applications," *Adv. Mater.*, vol. 24, no. 40, pp. 5408–5427, Oct. 2012.

[27] F. Menchini *et al.*, "Transparent hole-collecting and buffer layers for heterojunction solar cells based on n-type-doped silicon," *Appl. Phys. A*, vol. 124, no. 7, p. 489, Jul. 2018.

[28] A. S. Gudovskikh *et al.*, "n-GaP/p-Si Heterojunction Solar Cells Fabricated by PE-ALD," *Phys. status solidi c*, vol. 14, no. 10, Oct. 2017.

[29] J. Sheng *et al.*, "Improvement of the SiO_x Passivation Layer for High-Efficiency Si/PEDOT:PSS Heterojunction Solar Cells," *ACS Appl. Mater. Interfaces*, vol. 6, no. 18, pp. 16027–16034, Sep. 2014.

[30] J. Geissbühler *et al.*, "22.5% Efficient Silicon Heterojunction Solar Cell With Molybdenum Oxide Hole Collector," *Appl. Phys. Lett.*, vol. 107, no. 8, 2015.

[31] J. Bullock *et al.*, "Stable Dopant-Free Asymmetric Heterocontact Silicon Solar Cells with Efficiencies above 20%," *ACS Energy Lett.*, vol. 3, no. 3, pp. 508–513, Mar. 2018.

[32] W. Wu *et al.*, "22% efficient dopant-free interdigitated back contact silicon solar cells," in *AIP Conference Proceedings*, 2018, vol. 1999, no. 1, p. 40025.

[33] M. T. Greiner, M. G. Helander, W.-M. Tang, Z.-B. Wang, J. Qiu, and Z.-H. Lu, "Universal energy-level alignment of molecules on metal oxides," *Nat. Mater.*, vol. 11, no. 1, pp. 76–81, Jan. 2012.

[34] C. Battaglia *et al.*, "Silicon heterojunction solar cell with passivated hole selective MoO x contact," *Appl. Phys. Lett.*, vol. 104, no. 11, p. 113902, 2014.

[35] J. Bullock *et al.*, "E_cient silicon solar cells with dopant-free asymmetric heterocontacts," *Nat. Energy*, vol. 1, no. January, pp. 1–7, 2016.

[36] J. Meyer and A. L. Kahn, "Electronic structure of molybdenum-oxide films and associated charge injection mechanisms in organic devices," *J. Photonics Energy*, vol. 1, no. 1, p. 011109, Jan. 2011.

[37] M. Vasilopoulou *et al.*, "The In fl uence of Hydrogenation and Oxygen Vacancies on Molybdenum Oxides Work Function and Gap States for Application in Organic Optoelectronics," 2012.

[38] A. Cuevas *et al.*, "Carrier population control and

surface passivation in solar cells," *Sol. Energy Mater. Sol. Cells*, vol. 184, pp. 38–47, Sep. 2018.

[39] C. Ballif, A. Descoeudres, M. Despeisse, and S. De Wolf, "Advances in crystalline silicon heterojunction research and opportunities for low manufacturing costs," *2015 IEEE 42nd Photovolt. Spec. Conf. PVSC 2015*, pp. 1–5, 2015.

[40] D. Sacchetto *et al.*, "ITO/MoOx/a-Si:H(i) Hole-Selective Contacts for Silicon Heterojunction Solar Cells: Degradation Mechanisms and Cell Integration," *IEEE J. Photovoltaics*, vol. 7, no. 6, pp. 1584–1590, 2017.

[41] S. Essig *et al.*, "Toward Annealing-Stable Molybdenum-Oxide-Based Hole-Selective Contacts For Silicon Photovoltaics," *Sol. RRL*, vol. 2, no. 4, p. 1700227, Feb. 2018.

[42] J. Werner *et al.*, "Sputtered rear electrode with broadband transparency for perovskite solar cells," *Sol. Energy Mater. Sol. Cells*, vol. 141, 2015.

[43] J. H. Kim *et al.*, "The effect of Ar plasma bombardment upon physical property of tungsten oxide thin film in inverted top-emitting organic light-emitting diodes," *Org. Electron.*, vol. 12, no. 2, pp. 285–290, Feb. 2011.

[44] H. You, Y. Dai, Z. Zhang, and D. Ma, "Improved performances of organic light-emitting diodes with metal oxide as anode buffer," *J. Appl. Phys.*, vol. 101, no. 2, p. 026105, Jan. 2007.

[45] I.-M. Chan and F. C. Hong, "Improved performance of the single-layer and double-layer organic light emitting diodes by nickel oxide coated indium tin oxide anode," *Thin Solid Films*, vol. 450, no. 2, pp. 304–311, Mar. 2004.

[46] B. A. Kamino *et al.*, "Low-Temperature Screen-Printed Metallization for the Scale-Up of Two-Terminal Perovskite–Silicon Tandems," *ACS Appl. Energy Mater.*, p. acsaem.9b00502, May 2019.

[47] L. Lajaunie, F. Boucher, R. Dessapt, and P. Moreau, "Quantitative use of electron energy-loss spectroscopy Mo-M2,3 edges for the study of molybdenum oxides," *Ultramicroscopy*, vol. 149, pp. 1–8, 2015.

[48] H. Fujiwara and M. Kondo, "Effects of a-Si:H layer thicknesses on the performance of a-Si:H∕c-Si heterojunction solar cells," *J. Appl. Phys.*, vol. 101, no. 5, p. 054516, Mar. 2007.

[49] S. M. de Nicolás, D. Muñoz, A. S. Ozanne, N. Nguyen, and P. J. Ribeyron, "Optimisation of doped amorphous silicon layers applied to heterojunction solar cells," *Energy Procedia*, vol. 8, pp. 226–231, Jan. 2011.

[50] C. Battaglia *et al.*, "Silicon heterojunction solar cell with passivated hole selective MoO x contact," *Appl. Phys. Lett.*, vol. 104, no. 11, 2014.

[51] J. Bullock, A. Cuevas, T. Allen, and C. Battaglia, "Molybdenum oxide MoOx: A versatile hole contact for silicon solar cells," *Appl. Phys. Lett.*, vol. 105, no. 23, 2014.

[52] C. Messmer, M. Bivour, J. Schön, S. W. Glunz, and M. Hermle, "Numerical Simulation of Silicon Heterojunction Solar Cells Featuring Metal Oxides as Carrier-Selective Contacts," *Ieee J. Photovoltaics*, vol. 1, no. 2, pp. 1–9, Mar. 2018.

[53] E. T. Roe, K. E. Egelhofer, and M. C. Lonergan, "Exchange current density model for the contact-determined current-voltage behavior of solar cells," *J. Appl. Phys.*, vol. 125, no. 22, 2019.

[54] J. Haschke *et al.*, "Annealing of Silicon Heterojunction Solar Cells: Interplay of Solar Cell and Indium Tin Oxide Properties," *IEEE J. Photovoltaics*, vol. 9, no. 5, pp. 1202–1207, Sep. 2019.

[55] M. Boccard, C. Battaglia, F.-J. Haug, M. Despeisse, and C. Ballif, "Light trapping in solar cells: Analytical modeling," *Appl. Phys. Lett.*, vol. 101, no. 15, p. 151105, 2012.

[56] J. Haschke, C. Messmer, J. Cattin, M. Bivour, M. Boccard, and C. Ballif, "Injection-dependent lateral resistance in front-junction solar cells with nc-Si : H and a-Si : H hole selective contact," in *PVSC-46 Chicago*, 2019.